



**BUDAPEST UNIVERSITY OF TECHNOLOGY AND ECONOMICS**

**Faculty of Chemical Technology and Biotechnology**

**GYÖRGY OLÁH DOCTORAL SCHOOL**

**PhD Dissertation Title:**

Complex inverse opal photonic crystals for improved photocatalysis

**Thesis Booklet**

Author: Hamsasew Hankebo Lemago

Ph.D. Candidate at the Department of Inorganic and Analytical Chemistry,  
Budapest University of Technology and Economics (BME)

Supervisor: Prof. Dr. Imre Miklós Szilágyi (Professor, University of Miskolc,  
Institute of Physical Metallurgy, Metal Forming and Nanotechnology)

Internal Consultant: Dr. János Madarász (Associate professor, BME,  
Department of Inorganic and Analytical Chemistry)

November 2025

# 1. INTRODUCTION

Over recent years, semiconductor oxides (SCO) have garnered significant attention due to their versatile technological applications. Their non-toxic nature, chemical stability, and environmental benefits make them promising candidates for addressing pressing issues such as environmental pollution and the global energy crisis. They have been widely explored for various applications, including solar cells, UV Visible light emitters, fuel cells, batteries, transparent electronics, and photocatalysis [1,2]. In photocatalysis, the process involves light absorption, the generation and separation of electron-hole pairs, their migration to the photocatalyst's surface, and the subsequent redox reactions. Due to their high photoactivity, SCOs play a crucial role in photocatalyzing diverse reactions such as water splitting, pollutant degradation, energy conversion, environmental remediation, and self-cleaning surfaces. These properties make SCO-based photocatalysis a transformative approach for tackling environmental and energy-related challenges while offering new possibilities in chemical synthesis and materials science [3–5].

Inverse opal photonic crystal (IOPC) materials have emerged as a powerful strategy to enhance SCO-based photocatalysis by improving light-harvesting efficiency, charge transport, and reaction kinetics [6]. They are materials with a periodic variation in their refractive index, which allows for manipulating light propagation within the crystals. They are created by the inverse replication of a self-assembled template structure (for example, polymers, silica), resulting in an ordered array of voids or pores within a solid matrix. This distinctive structure gives inverse opal (IO) a range of interesting optical properties, making them attractive for various applications. The periodic arrangement of voids in IO materials gives rise to a photonic bandgap (PBG), a range of wavelengths that are forbidden to propagate through the material. This bandgap can be tuned by changing the spheres' size, shape, and composition, allowing for control over the material's optical properties [7–10].

Nanolithography and the self-assembly of colloidal microspheres are two prevalent techniques employed in fabricating IO structures. Nanolithography, referred to as the "top-down" approach, is relatively expensive and time-consuming, resulting in only a few structural layers of materials [11]. On the other hand, the "bottom-up" method, involving the self-assembly of colloidal microspheres, offers a cost-effective means of preparing crystalline samples comprising several hundred structural layers of varying thickness. In the bottom-up approach, various templates such as silica ( $\text{SiO}_2$ ), polystyrene (PS), or Polymethyl

methacrylate (PMMA) microspheres are meticulously arranged into an opal photonic crystal (PC) using methods like self-assembly [12], evaporation [13], stöber method [14], gravity sedimentation [15], and dip coating [16,17]. These opal PCs then serve as the templates into which the desired precursor or target material is introduced. Subsequently, the template is removed through calcination or etching, forming the IOPC. Throughout the preparation process, different methods can be employed to fill the precursor or target material, including Atomic Layer Deposition (ALD) [18], Chemical Vapor Deposition (CVD) [19], Electrochemical Deposition (ED) [20,21], sol-gel method [22,23], and more.

In this PhD study, I aimed to synthesize, analyse, and characterize ordered nanoporous IO structures composed of various oxides and their composites ( $\text{TiO}_2$ ,  $\text{ZnO}$ ,  $\text{Al}_2\text{O}_3$ ,  $\text{TiO}_2/\text{ZnO}$ ,  $\text{ZnO}/\text{TiO}_2$ ,  $\text{TiO}_2/\text{Al}_2\text{O}_3$ ,  $\text{ZnO}/\text{Al}_2\text{O}_3$ ,  $\text{Al}_2\text{O}_3/\text{TiO}_2$ ,  $\text{Al}_2\text{O}_3/\text{ZnO}$ ) using both ALD techniques via thermal ALD and plasma-enhanced ALD. My key objectives were to establish a controlled fabrication method for periodic polystyrene (PS) nanosphere sacrificial templates with diameters of 300 nm, 460 nm, and 600 nm through vertical layer deposition (VLD), which served as scaffolds for the subsequent ALD of IO oxides. These parameters critically influenced light localization and enhanced photocatalytic activity in the UV and visible range. Additionally, I explored different synthesis pathways using both PS suspensions and powders to optimize template ordering, morphology, and structural integrity. My goal was to engineer these nanostructured IO materials with tailored compositions and architectures to enhance their photocatalytic performance. Specifically, I fabricated both pristine and composite IOs by depositing the selected metal oxides onto PS templates of varying sizes, followed by template removal via annealing.

I first focused on synthesizing  $\text{TiO}_2$ ,  $\text{ZnO}$ , and  $\text{TiO}_2/\text{ZnO}$  IO structures using PS-300 templates to maximize PBG effects in the UV Visible region and enhance their photocatalytic activities. I then investigated  $\text{Al}_2\text{O}_3$ -based IO structures and their composites ( $\text{Al}_2\text{O}_3/\text{ZnO}$  and  $\text{Al}_2\text{O}_3/\text{TiO}_2$ ) using PS-460 templates, comparing TALD and PEALD techniques to evaluate their influence on film quality, surface morphology, and defect passivation. Finally, I extended the study to PS-600-templated  $\text{ZnO}$  and  $\text{TiO}_2$  IOs coated with ultrathin  $\text{Al}_2\text{O}_3$  layers to fabricate bilayer structures aimed at improving photocatalytic activity under UV and visible light. After preparing the IO materials, I conducted a comprehensive characterization of their structural, compositional, and optical properties using techniques such as Scanning Electron Microscope/Energy Dispersive X-ray Spectroscopy (SEM/EDX), Atomic Force Microscopy (AFM), X-ray Diffraction (XRD), Raman spectroscopy, X-ray Photoelectron Spectroscopy

(XPS), Photoluminescence (PL), and UV Visible spectroscopy. These analyses confirmed the crystalline structures of ZnO and TiO<sub>2</sub> and the amorphous nature of Al<sub>2</sub>O<sub>3</sub>. I also evaluated their photocatalytic performance under UV and visible light by testing the degradation of methylene blue (MB), rhodamine 6G (Rh6G), and 4-nitrophenol (4NP).

## **2. EXPERIMENTAL**

### **2.1. Preparation of Polystyrene Nanosphere Opal Template**

The opal template was prepared from PS suspensions with different particle sizes (Sigma Aldrich, 10% w/w and 300, 460, or 600 nm particle size) diluted to 3.0% (V/V). For the preparation of the PS suspension, 15 mg of PS powder was mixed with 4.85 ml of ion exchange water and stirred manually. An ultrasonication was performed to enhance particle uniformity. The resulting PS suspension was then used to grow an opal layer on a microscope glass slide using the VLD. After ultrasonication, the suspension was placed in a closed container to prevent evaporation. Cleaned glass slides, treated with the so-called “piranha solution” (a mixture of 98% (v/v) H<sub>2</sub>SO<sub>4</sub> and 30% (w/w) H<sub>2</sub>O<sub>2</sub> in a 3:1 ratio) to enhance hydrophilicity, were placed at a 45-degree angle in the PS suspension to facilitate vertical deposition. The slides were then placed in a furnace at 50°C for 14 hours, followed by heating at 80°C for 90 minutes, allowing the colloidal crystal to form through self-assembly during water evaporation.

### **2.2. Thin Film Deposition Using ALDs**

The ALD methods, known as TALD and PEALD, were utilized to produce IOPC materials. TALD utilizes thermal energy for surface reactions, while PEALD employs plasma to enhance reactivity and control film properties at lower temperatures. PEALD utilizes plasma species as a co-reactant to enhance precursor reactivity, enabling the growth of high-quality films at low temperatures. The process involves preheating the ALD chamber to 50 °C, followed by inserting samples and a reference silicon wafer into the reactor. For the deposition processes, TiCl<sub>4</sub>, DEZ, and TMA were used as precursors for TiO<sub>2</sub>, ZnO, and Al<sub>2</sub>O<sub>3</sub>, respectively, with H<sub>2</sub>O serving as the oxidizing agent. For example, in the case of TiO<sub>2</sub>, each ALD cycle comprised a 0.3 s TiCl<sub>4</sub> pulse, followed by a 3 s N<sub>2</sub> purge, a 0.3 s H<sub>2</sub>O pulse, and a subsequent 3 s N<sub>2</sub> purge. These depositions were carried out at a controlled temperature of 52.9°C in thermal mode.

### 3. RESULTS AND ANALYSIS

#### 3.1. Synthesis of TiO<sub>2</sub> IO, ZnO IO, ZnO/TiO<sub>2</sub>, and TiO<sub>2</sub>/ZnO composites via PEALD

This study introduced a synthesis approach to enhancing photocatalytic efficiency by synthesizing TiO<sub>2</sub>/ZnO and ZnO/TiO<sub>2</sub> IO structures using PEALD. Successfully fabricated ordered and interconnected porous architectures employing 300 nm-sized PS templates through a low-temperature process. Characterization techniques, including SEM (Fig. 3.1 a & b), XRD, Raman spectroscopy, and UV-Vis spectroscopy (Fig. 3.1 c), confirmed the formation of IOs with ordered structures, controlled crystallinity, and distinct PBGs within the visible region. The presence of these PBGs resulted in the "slow photon" effect, significantly enhancing light-matter interactions within the IO structures. Pristine TiO<sub>2</sub> and ZnO IOs exhibited better photocatalytic activity under UV light for degrading pollutants such as 4NP and Rh6G (Fig. 3.1 d). This performance was attributed to several factors: 1) their high periodicity and hollow IO structure, which provided ample active sites for pollutant adsorption; 2) their bandgap alignment (3.0 eV for TiO<sub>2</sub> and 3.2 eV for ZnO), enabling efficient absorption of UV photons and subsequent generation of electron-hole pairs; and 3) optimized charge carrier dynamics within the pristine IO structures.

Conversely, composite IOs (TiO<sub>2</sub>/ZnO and ZnO/TiO<sub>2</sub>) demonstrated significantly enhanced photocatalytic activity under visible light irradiation. This improved performance was attributed to a synergistic effect between 1) band gap modulation, where the combination of TiO<sub>2</sub> and ZnO allowed for broader light absorption across the visible spectrum. Furthermore, the precise control over layer thicknesses and morphologies achieved through the PEALD technique contributed to improved light trapping and efficient charge carrier transport within the composite IO structures.

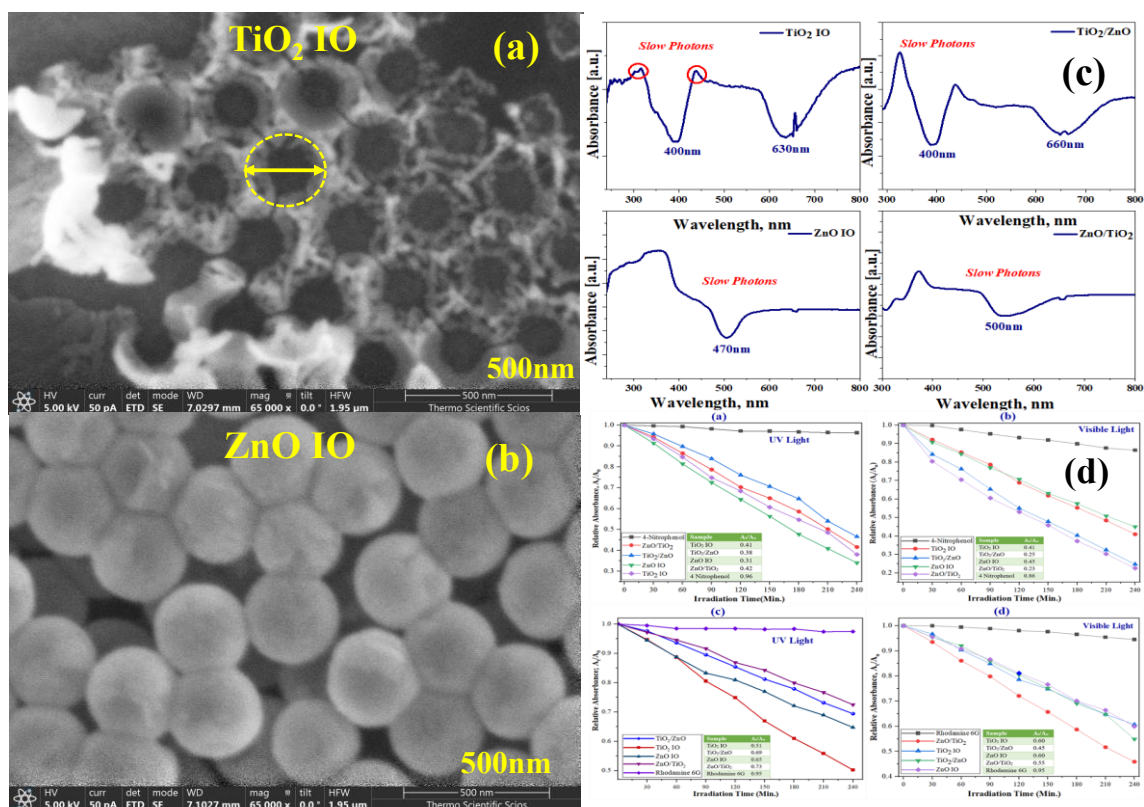


Figure 3.1: SEM images of pure IOs (a and b), UV Visible spectroscopy (c), and photocatalytic results of pure  $\text{TiO}_2$  IO, pure  $\text{ZnO}$  IO, and their composites ( $\text{TiO}_2/\text{ZnO}$ , and  $\text{ZnO}/\text{TiO}_2$ ) under UV and visible light with Rh6G and 4NP pollutants (d), respectively.

### 3.2. Synthesis of $\text{Al}_2\text{O}_3$ IO and its composites via TALD and PEALD Methods

This study determined the synthesis and characterization of IOPCs composed of  $\text{Al}_2\text{O}_3$  and its composites, coated with ultra-thin  $\text{ZnO}$  and  $\text{TiO}_2$  layers using TALD and PEALD. The study also demonstrated the successful fabrication of IOPC structures using 460 nm-sized PS nanospheres as a template, followed by  $\text{Al}_2\text{O}_3$  infiltration and template removal. Characterization techniques, including SEM, EDX, TG, UV Visible spectroscopy, AFM, PL, and XPS, confirmed the periodic, interconnected IO structures and the successful incorporation of  $\text{ZnO}$  and  $\text{TiO}_2$  layers. TALD resulted in smoother surfaces compared to PEALD (Fig. 3.2 a and b), while UV Visible spectroscopy (Fig. 3.2 c) revealed absorption peaks related to the PBG and “slow photon” effects. Despite an annealing temperature of  $900^\circ\text{C}$ , the final  $\text{Al}_2\text{O}_3$  IO and its composites exhibited an amorphous structure. PL analysis showed that the incorporation of  $\text{ZnO}$  and  $\text{TiO}_2$  layers, particularly with PEALD, enhanced PL intensity by passivating defects and improving optical properties. XPS analysis confirmed the presence of

$\text{Al}_2\text{O}_3$ ,  $\text{ZnO}$ , and  $\text{TiO}_2$ , along with oxygen vacancies and aluminum hydroxide formation, indicating successful material incorporation (Fig. 3.2 d).

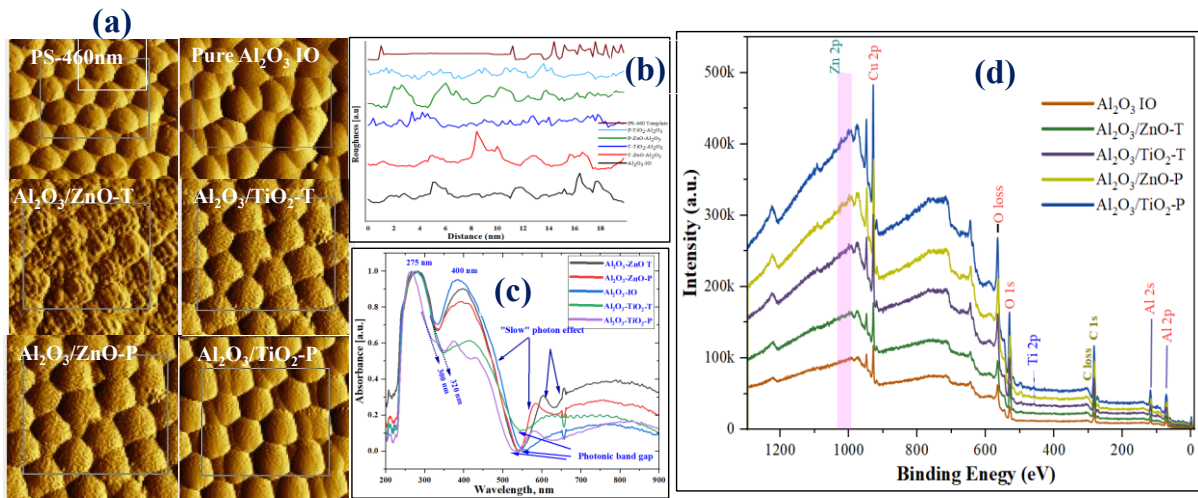


Figure 3.2. AFM images of the ALD grown samples: (a), Roughness of the materials by AFM (b), UV Visible spectra (c), and XPS result of  $\text{Al}_2\text{O}_3$  IO and its composite materials (d), respectively.

### 3.3. Synthesis of $\text{ZnO}$ IO and $\text{ZnO}/\text{Al}_2\text{O}_3$ Composites via TALD and PEALD

This study also details the synthesis and characterization of  $\text{ZnO}$  IOs and  $\text{ZnO}/\text{Al}_2\text{O}_3$  composites utilizing ALD methods, specifically TALD and PEALD (Fig. 3.3a). A 600 nm PS nanosphere template was employed to create the periodic IO structure, followed by  $\text{ZnO}$  deposition and subsequent annealing at  $500^\circ\text{C}$  to remove the template. Ultra-thin  $\text{Al}_2\text{O}_3$  films were grown on  $\text{ZnO}$  IOs via TALD and PEALD. Characterization techniques, including SEM (Fig. 3.3 b), XRD (Fig. 3.4a), UV-Vis spectroscopy (Fig. 3.4 b), PL analysis (Fig. 3.4 c), and so on were confirmed the wurtzite  $\text{ZnO}$  IO structure and the amorphous nature of the  $\text{Al}_2\text{O}_3$  layers. The study highlighted the role of photonic crystal effects, including “slow photons” and PBG shifts, in enhancing light absorption and photocatalytic efficiency. The photocatalytic activity was evaluated using MB, Rh6G, and NP. While the pristine  $\text{ZnO}$  IO structure demonstrated effective MB degradation due to efficient light capture, its performance decreased with Rh6G and 4-NP. The  $\text{ZnO}/\text{Al}_2\text{O}_3$ -TALD composite exhibited superior photocatalytic performance compared to pristine IO and  $\text{ZnO}/\text{Al}_2\text{O}_3$ -PEALD composites, achieving the fastest degradation rates for MB and Rh6G. This enhancement is attributed to factors such as the passivation effect of the  $\text{Al}_2\text{O}_3$  layer, the preservation of the highly ordered IO structure, and the controlled introduction of defects. In contrast, the PEALD-coated

composite showed reduced activity due to increased disorder and defects introduced by the plasma-assisted deposition process.

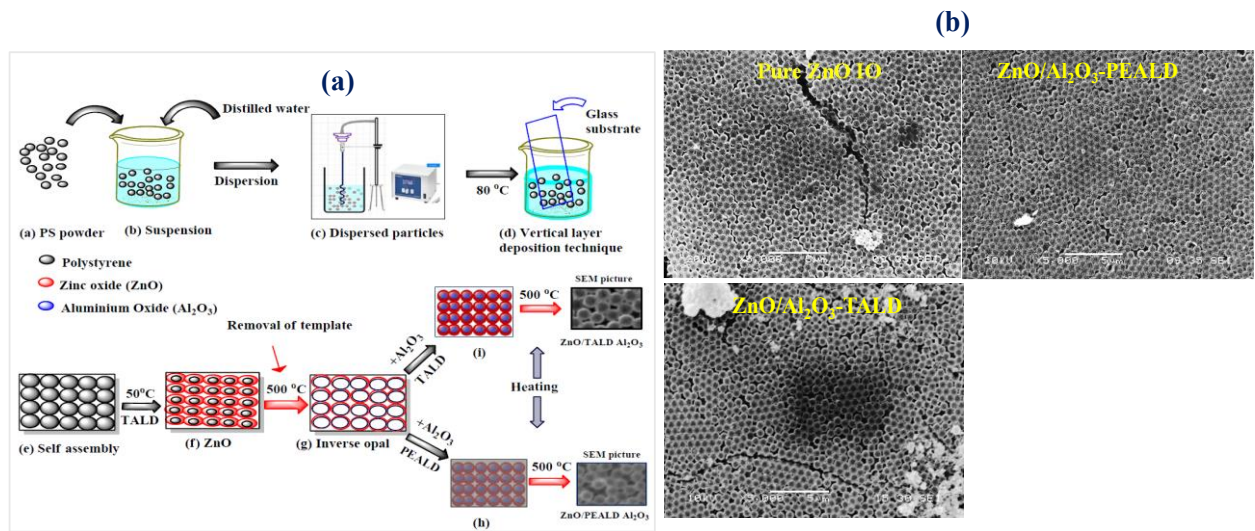


Figure 3.3: Synthesis of paths (a) of ZnO IO and ZnO/Al<sub>2</sub>O<sub>3</sub> composite structures using TALD and PEALD techniques, and (b) SEM images of ZnO IO, ZnO/Al<sub>2</sub>O<sub>3</sub>-TALD, and ZnO/Al<sub>2</sub>O<sub>3</sub>-PEALD composites, respectively.

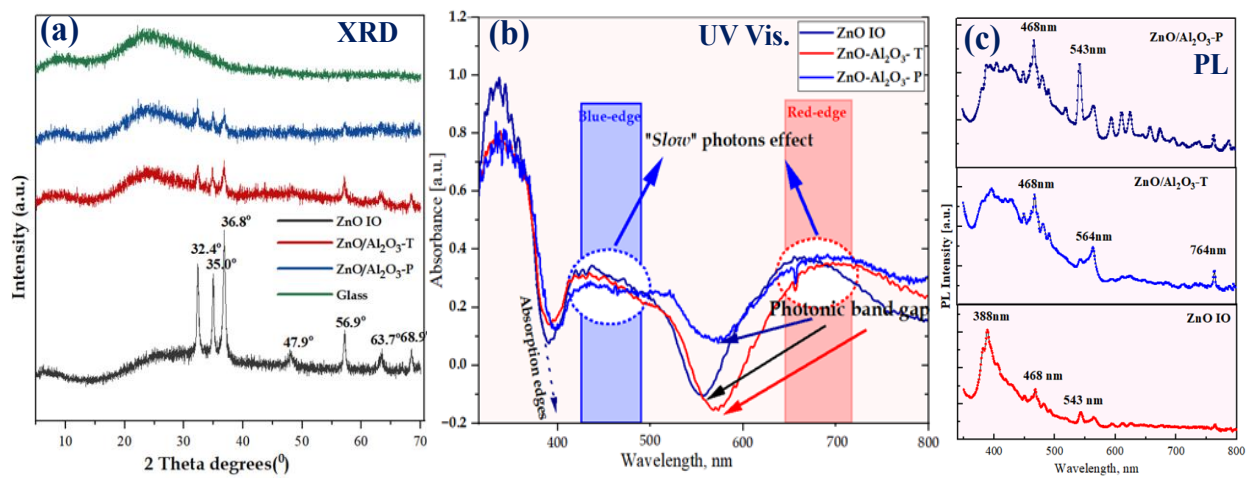


Figure 3.4: XRD patterns (a), UV visible, and PL spectroscopy (b), for ZnO IO, ZnO/Al<sub>2</sub>O<sub>3</sub>-T, and ZnO/Al<sub>2</sub>O<sub>3</sub>-P (c), respectively.

### 3.4. Synthesis of TiO<sub>2</sub> IO, and TiO<sub>2</sub>/Al<sub>2</sub>O<sub>3</sub> composites via TALD and PEALD

This study successfully synthesized TiO<sub>2</sub> IO and ultra-thin films of Al<sub>2</sub>O<sub>3</sub> on composite IOs using TALD or PEALD and VLD from a 600 nm-sized PS nanosphere opal template. The results showed that the highly ordered opal crystal macrostructure had a face-centered cubic (FCC) orientation. The proposed annealing temperature (500 °C) efficiently removed the

template, leaving the anatase phase IO, which provided a small contraction in the spheres. In comparison to  $\text{TiO}_2/\text{Al}_2\text{O}_3$  PEALD,  $\text{TiO}_2/\text{Al}_2\text{O}_3$  TALD had a better charge interaction of photoexcited electron-hole pairs in the valence band hole to restrain recombination, resulting in a broad spectrum with a peak in the green region. This was demonstrated by PL (Fig. 3.5 a). Strong absorption bands were found in the UV regions, including increased absorption due to “slow photons” and a narrow optical band gap in the visible region. The results from the photocatalytic activity of the samples showed decomposition rates of 35.4%, 24.7%, and 14.8%, for  $\text{TiO}_2$ ,  $\text{TiO}_2/\text{Al}_2\text{O}_3$  (Fig. 3.5 b), TALD, and PEALD IO ALD samples, respectively. The result showed that ultrathin amorphous ALD-grown  $\text{Al}_2\text{O}_3$  layers had considerable photocatalytic activity. The  $\text{Al}_2\text{O}_3$  thin film grown by TALD had a more ordered structure than the plasma ALD-prepared one, explaining its higher photocatalytic activity. The declined photocatalytic activity of the combined layers was observed due to the reduced electron tunneling effect resulting from the thinness of  $\text{Al}_2\text{O}_3$ .

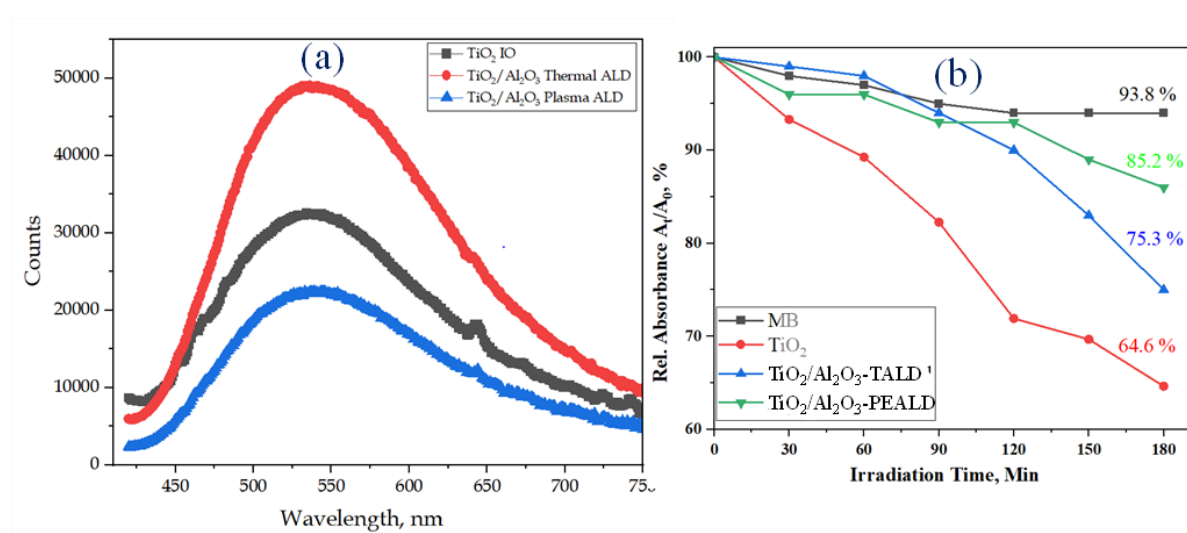


Figure 3.5: (a) PL analysis results, and (b) photocatalysis  $\text{TiO}_2$  IO and its composites, respectively.

#### 4. POSSIBLE APPLICATIONS OF RESULTS

Using TALD and PEALD, this study shows exact control over the morphology and optical quality of IOPCs, enabling tunable PBGs and "slow photon" effects that are essential for advanced photonic devices and solar energy harvesting. The synthesis technique and template size (300–600 nm) can be changed to optimise light capture or align the optical response with pollutant absorption spectra. Double-layer composites, such as  $\text{TiO}_2/\text{Al}_2\text{O}_3$  and  $\text{ZnO}/\text{Al}_2\text{O}_3$ , showed significantly enhanced photocatalytic performance by suppressing charge recombination and improving pollutant degradation under UV or Visible light. Furthermore, it was discovered that the deposition order was critical, with  $\text{TiO}_2/\text{ZnO}$  outperforming  $\text{ZnO}/\text{TiO}_2$ , highlighting the significance of interfacial engineering for effective environmental remediation. ALD-fabricated IOPCs are promising platforms for solar energy conversion, water purification, gas sensing, selective adsorption, and even as frameworks for high-performance lithium-ion batteries due to their structural integrity and tunability, which extend beyond photocatalysis. These results demonstrate their potential in environmentally friendly and sustainable energy technologies.

## 5. THESIS POINTS

1. Using low-temperature (50 °C) plasma-enhanced atomic layer deposition (PEALD), I synthesized TiO<sub>2</sub> and ZnO single-material as well as ZnO/TiO<sub>2</sub> and TiO<sub>2</sub>/ZnO composite inverse opal photonic crystal (IOPC) structures. For this opal template of 300 nm sacrificial polystyrene (PS) particles were applied, which were removed after PEALD by annealing in air at 500 °C. The second PEALD layer resulted in a ca. 30 nm red shift in the photonic bandgap (PBG) compared to the PBG of the first layer. In photocatalytic tests, single-material IOPCs degraded the model pollutants (4-nitrophenol, 4-NP and rhodamine 6G, Rh6G) more efficiently under UV light, while the composites were more efficient under visible-light irradiation [P3].
2. I prepared Al<sub>2</sub>O<sub>3</sub>/TiO<sub>2</sub> and Al<sub>2</sub>O<sub>3</sub>/ZnO IOPCs using a combination of thermal atomic layer deposition (TALD) and PEALD. At first, Al<sub>2</sub>O<sub>3</sub> IOPC was made via TALD using a 460 nm PS opal template, depositing 36 nm Al<sub>2</sub>O<sub>3</sub> layer by TALD and annealing it at 450 °C. Then ultrathin (~5 nm) TiO<sub>2</sub> or ZnO overlayers were grown by both TALD and PEALD on the Al<sub>2</sub>O<sub>3</sub> IOPC to form Al<sub>2</sub>O<sub>3</sub>/TiO<sub>2</sub> and Al<sub>2</sub>O<sub>3</sub>/ZnO composites, followed by post annealing at 900 °C. Atomic force microscopy (AFM) showed that composites with TALD-grown overlayers had smoother surfaces (Root mean square - RMS: 17–18 nm) than those grown by PEALD (RMS: 19–20 nm) [P4].
3. I fabricated ZnO/Al<sub>2</sub>O<sub>3</sub> IOPCs by combining TALD and PEALD. A 52 nm ZnO layer was first grown by TALD on a 600 nm PS nanosphere opal template and subsequently converted into a ZnO IOPC by annealing at 500 °C. Consecutively, an ultrathin (~5 nm) Al<sub>2</sub>O<sub>3</sub> layer was deposited by TALD or PEALD to obtain ZnO/Al<sub>2</sub>O<sub>3</sub>-TALD and ZnO/Al<sub>2</sub>O<sub>3</sub>-PEALD composites. The electric bandgap shifted from 3.3 ± 0.01 eV (single-material ZnO) to 3.4 ± 0.01 eV for TALD-coated and 3.6 ± 0.01 eV for PEALD-coated composites, due to the ultrathin Al<sub>2</sub>O<sub>3</sub> overlayer. After 3 hours visible-light irradiation the TALD-coated composite was more effective in the photocatalytic decomposition of photocatalytic studies to decompose methylene blue (MB), Rh6G, and 4-NP model compounds, achieving 69 %, 40 %, and 27 % degradation, respectively, compared to the PEALD-coated composite (48 %, 23 %, and 22 % degradation, respectively) [P2].

4. By combining TALD and PEALD, I synthesized  $\text{TiO}_2/\text{Al}_2\text{O}_3$  IOPCs. At first,  $\text{TiO}_2$  IOPC was prepared by depositing 52 nm of  $\text{TiO}_2$  via TALD onto a 600 nm PS sacrificial template, followed by annealing at 500 °C. After this, a ~5 nm  $\text{Al}_2\text{O}_3$  film was grown on it by either TALD or PEALD to get  $\text{TiO}_2/\text{Al}_2\text{O}_3$ -TALD and  $\text{TiO}_2/\text{Al}_2\text{O}_3$ -PEALD composites. The electric bandgap ( $3.2 \pm 0.01$  eV for the  $\text{TiO}_2$ ) shifted to  $3.6 \pm 0.01$  eV for TALD-coated, and to  $3.8 \pm 0.01$  eV for PEALD-coated composites, due to the ultrathin  $\text{Al}_2\text{O}_3$  overlayer. The TALD composite exhibited more efficient photocatalytic activity than its PEALD counterpart, achieving 25% MB degradation under 3 hours of visible-light irradiation, compared to 15% [P1].

## 6. PUBLICATIONS

### 6.1. PUBLICATIONS RELATED TO DISSERTATION

- P1 **Hamsasew Hankebo Lemago**, Addin F.S., Atilla K, Igricz T, Parditka B, Hessz D, Erdélyi Z., Szilagyi I.M., Synthesis of TiO<sub>2</sub>/Al<sub>2</sub>O<sub>3</sub> Double-layer inverse opal by thermal and plasma-assisted atomic layer deposition for photocatalytic applications. *Nanomaterials* **2023**, 13, 1314. <https://doi.org/10.3390/nano13081314>; **Q1**, IF:**4.4**, Independent Citations: 1.
- P2 **Hamsasew Hankebo Lemago**, Nour Khauli, Dóra Hessz, Tamás Igricz, Pál Petra, Csaba Cserhádi, Baradács Eszter Mónika, Bence Parditka, Zoltán Erdélyi, Imre Miklós Szilágyi, Fabrication of ZnO/Al<sub>2</sub>O<sub>3</sub> inverse opals with atomic layer deposited Amorphous-Al<sub>2</sub>O<sub>3</sub> for enhanced photocatalysis. *Materials Science in Semiconductor Processing* **2024**, 183, 108733. <https://doi.org/10.1016/j.mssp.2024.108733>; **Q1**, IF: **4.2**, Independent Citations: 3.
- P3 **Hamsasew Hankebo Lemago**, Letícia Tolezani, Tamás Igricz, Dóra Hessz, Petra Pál, Csaba Cserhádi, Gergő Vecsei, Barbara Sárközi, Eszter Mónika Baradács, Zoltán Erdélyi, and Imre Miklós Szilágyi, Enhanced Photocatalysis via Inverse Opal Structures: Synthesis and Characterization of TiO<sub>2</sub>/ZnO and ZnO/TiO<sub>2</sub> Composites Using Plasma-Enhanced ALD. *Ceramic International* **2025**, 51, 339352. <https://doi.org/10.1016/j.ceramint.2024.10.465>; **Q1**, IF: **5.1**, Independent Citations: 17.
- P4 **Hamsasew Hankebo Lemago**, Soeun Choi, Dóra Hessz, Gyula Jággerszki, Petra Pál, Csaba Cserhádi, Eszter Mónika Baradács, Tamás Fodor, Zoltán Erdélyi, and Imre Miklós Szilágyi, Thermal, and Plasma-Enhanced ALD for the Synthesis of Inverse Opal Al<sub>2</sub>O<sub>3</sub> and Its Composite Materials. *Vacuum*, **2025**, 238, 114254. <https://doi.org/10.1016/j.vacuum.2025.114254>; **Q1**, IF: **3.8**, Independent Citations: 0.

## 6.1. PUBLICATION PARTLY RELATED TO DISSERTATION

1. **Hamsasew Hankebo Lemago**, and Imre Miklós Szilágyi, Inverse opal photonic crystals: synthesis techniques, unique properties, and multifunctional applications, A review paper, *Applied Surface Science Advances* **2025** 28,100805. <https://doi.org/10.1016/j.apsadv.2025.100805>, SJR 2024, **Q1**, IF: **8.7**, Independent Citations: 0.

## 6.2. PUBLICATION NOT RELATED TO DISSERTATION

1. Luminița Predoană, Jeanina Pandele-Cusu, Irina Atkinson, Simona Petrescu, Oana Cătălina Mocioiu, Daniela C. Culiță, Dániel Attila Karajz, Vincent Otieno Odhiambo, **Hamsasew Hankebo Lemago**, Ana Paula Barreto Gomes, Zalán István Várady, Marcell Bohus, Imre M. Szilágyi, György Pokol, Ruxandra M. Costescu, Maria Zaharescu; Comparative study of the Cu-TiO<sub>2</sub> nanostructures obtained by sol-gel and microwave-assisted sol-gel methods; *Journal of Sol-Gel Science and Technology*, 2025, 114, 965–982. <https://doi.org/10.1007/s10971-025-06757-x>, SJR 2024, **Q2**, IF: **2.3**, Independent Citations: 0.

## 7. CONFERENCE PARTICIPATION

1. **Hamsasew Hankebo Lemago**, Feras Shugaa Addin, Bence Parditka, Zoltán Erdélyi, and Imre Miklós Szilágyi; 11–13<sup>th</sup> of July **2022**, 1st Forum of Young Researchers on Heterogeneous Catalysis, YOURHETCAT 2022, Szeged, Hungary; **Poster** presentation on Preparation of TiO<sub>2</sub>/Al<sub>2</sub>O<sub>3</sub> double-layered inverse opal photocatalysts by plasma and thermal ALD methods.
2. **Hamsasew Hankebo Lemago**, Daniel Karajz, Nour Khauli, Tamas Igricz, Bence Parditka, Zoltán Erdélyi and Imre Miklós Szilágyi; 26<sup>th</sup> of September **2022**, 4<sup>th</sup> George Olah Conference, Budapest Hungary. **Poster** presentation on Fabrication and characterization of ZnO and ZnO/Al<sub>2</sub>O<sub>3</sub> composite inverse opals by thermal and plasma-assisted ALD for photocatalysis.
3. **Hamsasew Hankebo Lemago**, Tamás Igricz, Bence Parditka, Zoltán Erdélyi, and Imre Miklós Szilágyi; 3<sup>rd</sup> Journal of Thermal Analysis and Calorimetry Conference and 9<sup>th</sup> V4 (Joint Czech-Hungarian-Polish-Slovakian) Thermoanalytical Conference 20–23<sup>rd</sup> June 2023, Balatonfüred, Hungary, **Poster** presentation on Thermal and plasma-assisted atomic layer deposition for the synthesis of inverse opal photocatalysts.
4. **Hamsasew Hankebo Lemago**, L. Tolezani, A. Choi, T. Igricz, B. Parditka, Z. Erdélyi, and I.M. Szilágyi, International Conference of Physical Chemistry - ROMPHYSICHEM 17th

edition: September 25-27, **2023**, Bucharest, Romania, **Oral** presentation, ZnO-Al<sub>2</sub>O<sub>3</sub> composite inverse opals for enhanced Photocatalysis.

5. **Hamsasew Hankebo Lemago**, Tamás Igricz, Zoltán Erdélyi, and Imre Miklós Szilágyi, Materials science day XXIII of PhD students" conference on the 20<sup>th</sup> November **2023**, Veszprém, Materials science day XXIII of PhD students" conference on the 20<sup>th</sup> November 2023, Veszprém, **Oral** presentation, Atomic Layer Deposition of Inverse Opals for Photocatalytic Degradation of Methylene Blue under Visible Light Illumination,
6. Cristina Maria Vlăduț, Oana Cătălina Mocioiu, Irina Atkinson, Imre Miklós Szilágyi, Jeanina Pandeale Cușu, János Madarász, Dániel Karajz, **Hamsasew Hankebo Lemago**; 3<sup>rd</sup> Journal of Thermal Analysis and Calorimetry Conference and 9th V4 (Joint: Czech-Hungarian-Polish-Slovakian) Thermoanalytical Conference 20–23<sup>rd</sup> June **2023**, Balatonfüred, Hungary, **Poster** presentation, Synthesis and Characterization of Doped Zinc Oxide Nanoparticles for Nanofluids.
7. Luminita Predoana, Irina Atkinson, Dániel Attila Karajz, Vincent Otieno Odhiambo, **Hamsasew Hankebo Lemago**, Jeanina Pandeale-Cusu, Simona Petrescu, Adriana Rusu, Nicoleta Apostol, Imre M. Szilágyi, György Pokol, Maria Zaharescu, July 24-29 International Solgel Conference Sol-gel **2022**, Lyon, France. **Poster** presentation, Properties of the Cu-TiO<sub>2</sub> nanostructures obtained by sol-gel and microwave-assisted sol-gel methods.

## 8. REFERENCES

- [1] J. Theerthagiri, S.J. Lee, K. Karuppasamy, S. Arulmani, S. Veeralakshmi, M. Ashokkumar, M.Y. Choi, Application of advanced materials in sonophotocatalytic processes for the remediation of environmental pollutants, *J. Hazard. Mater.* 412 (2021) 125245. <https://doi.org/10.1016/j.jhazmat.2021.125245>.
- [2] C. Karthikeyan, P. Arunachalam, K. Ramachandran, A.M. Al-Mayouf, S. Karuppuchamy, Recent advances in semiconductor metal oxides with enhanced methods for solar photocatalytic applications, *J. Alloys Compd.* 828 (2020) 154281. <https://doi.org/10.1016/j.jallcom.2020.154281>.
- [3] L. Zhu, X. Shang, K. Lei, C. Wu, S. Zheng, C. Chen, H. Song, Doping in Semiconductor Oxides-Based Electron Transport Materials for Perovskite Solar Cells Application, *Sol. RRL.* 5 (2021). <https://doi.org/10.1002/solr.202000605>.
- [4] A. Chaudhari, X. Cui, B. Hoex, L. Hyde, C.N. Ironside, W.M. Jadwisienczak, M.E. Kordesch, F. Rahman, R.D. Vispute, Zinc oxide family semiconductors for ultraviolet radiation emission – A cathodoluminescence study, *Mater. Res. Bull.* 153 (2022) 111906. <https://doi.org/10.1016/j.materresbull.2022.111906>.
- [5] M.I. Din, R. Khalid, Z. Hussain, Recent Research on Development and Modification of Nontoxic Semiconductor for Environmental Application, *Sep. Purif. Rev.* 50 (2021) 244–261. <https://doi.org/10.1080/15422119.2020.1714658>.
- [6] E. Armstrong, C. O'Dwyer, Artificial opal photonic crystals and inverse opal structures-fundamentals and applications from optics to energy storage, *J. Mater. Chem. C.* 3 (2015) 6109–6143. <https://doi.org/10.1039/c5tc01083g>.
- [7] Z. Li, M. Xiao, Y.F. Liu, H.H. Gao, P. V. Braun, Three-dimensional mesostructured binder-free nickel-based TiO<sub>2</sub>/RGO lithium-ion battery negative electrodes with enhanced volumetric capacity, *Ceram. Int.* 47 (2021) 21381–21387. <https://doi.org/10.1016/j.ceramint.2021.04.147>.
- [8] B.H. Patil, K. Jang, S. Lee, J.H. Kim, C.S. Yoon, J. Kim, D.H. Kim, H. Ahn, Periodically ordered inverse opal TiO<sub>2</sub>/polyaniline core/shell design for electrochemical energy storage applications, *J. Alloys Compd.* 694 (2017) 111–118. <https://doi.org/10.1016/j.jallcom.2016.09.331>.

- [9] J. Jiang, C. Li, S. Zhu, Z. Chen, M. Fu, D. He, Y. Wang, Optical properties of PMMA inverse opal structures with anisotropic geometries by stretching, *Mater. Res. Express.* 7 (2020) 0–6. <https://doi.org/10.1088/2053-1591/ab88fe>.
- [10] A. Lonergan, D. McNulty, C. O'Dwyer, Tetrahedral framework of inverse opal photonic crystals defines the optical response and photonic band gap, *J. Appl. Phys.* 124 (2018). <https://doi.org/10.1063/1.5033367>.
- [11] N. Abid, A.M. Khan, S. Shujait, K. Chaudhary, M. Ikram, M. Imran, J. Haider, M. Khan, Q. Khan, M. Maqbool, Synthesis of nanomaterials using various top-down and bottom-up approaches, influencing factors, advantages, and disadvantages: A review, *Adv. Colloid Interface Sci.* 300 (2022) 102597. <https://doi.org/10.1016/j.cis.2021.102597>.
- [12] H. Shahi, J. Kaur, S. Vaidya, Designing Nanostructured Materials through Self-Assembly and their Applications, *J. Inst. Eng. Ser. C.* 103 (2022) 135–142. <https://doi.org/10.1007/s40032-021-00660-4>.
- [13] J.E.S. Van Der Hoeven, A. V. Shneidman, N.J. Nicolas, J. Aizenberg, Evaporation-Induced Self-Assembly of Metal Oxide Inverse Opals: From Synthesis to Applications, *Acc. Chem. Res.* 55 (2022) 1809–1820. <https://doi.org/10.1021/acs.accounts.2c00087>.
- [14] D.A. Santamaría Razo, L. Pallavidino, E. Garrone, F. Geobaldo, E. Descrovi, A. Chiodoni, F. Giorgis, A version of Stöber synthesis enabling the facile prediction of silica nanospheres size for the fabrication of opal photonic crystals, *J. Nanoparticle Res.* 10 (2008) 1225–1229. <https://doi.org/10.1007/s11051-008-9373-4>.
- [15] F. Meseguer, A. Blanco, H. Míguez, F. García-Santamaría, M. Ibisate, C. López, Synthesis of inverse opals, *Colloids Surfaces A Physicochem. Eng. Asp.* 202 (2002) 281–290. [https://doi.org/10.1016/S0927-7757\(01\)01084-6](https://doi.org/10.1016/S0927-7757(01)01084-6).
- [16] B.Y. Valles-Pérez, M.A. Badillo-Ávila, G. Torres-Delgado, R. Castanedo-Pérez, O. Zelaya-Ángel, Photocatalytic activity of ZnO + CuO thin films deposited by dip coating: coupling effect between oxides, *J. Sol-Gel Sci. Technol.* 93 (2020) 517–526. <https://doi.org/10.1007/s10971-020-05223-0>.
- [17] C.C. Chiang, L.D. Tuyen, C.R. Ren, L.K. Chau, C.Y. Wu, P.J. Huang, C.C. Hsu, Fabrication of titania inverse opals by multi-cycle dip-infiltration for optical sensing, *Photonics Nanostructures - Fundam. Appl.* 19 (2016) 48–54.

<https://doi.org/10.1016/j.photonics.2016.02.004>.

- [18] A. Di Mauro, M.E. Fragalà, V. Privitera, G. Impellizzeri, ZnO for application in photocatalysis: From thin films to nanostructures, *Mater. Sci. Semicond. Process.* 69 (2017) 44–51. <https://doi.org/10.1016/j.mssp.2017.03.029>.
- [19] L. Sun, G. Yuan, L. Gao, J. Yang, M. Chhowalla, M.H. Gharahcheshmeh, K.K. Gleason, Y.S. Choi, B.H. Hong, Z. Liu, Chemical vapour deposition, *Nat. Rev. Methods Prim.* 1 (2021). <https://doi.org/10.1038/s43586-020-00005-y>.
- [20] Y. Zhou, J. Zhao, Y. Liu, R.J.H. Ng, J.K.W. Yang, Optical and electrochemical properties of 3D nanoporous Cu<sub>2</sub>O–Cu inverse opal structures tuned by electrodeposition, *Mater. Sci. Semicond. Process.* 121 (2021). <https://doi.org/10.1016/j.mssp.2020.105444>.
- [21] S. Koussi-Daoud, O. Majerus, D. Schaming, T. Pauporté, Electrodeposition of NiO Films and Inverse Opal Organized Layers from Polar Aprotic Solvent-Based Electrolyte, *Electrochim. Acta.* 219 (2016) 638–646. <https://doi.org/10.1016/j.electacta.2016.10.074>.
- [22] V. Abramova, A. Sinitskii, Large-scale ZnO inverse opal films fabricated by a sol-gel technique, *Superlattices Microstruct.* 45 (2009) 624–629. <https://doi.org/10.1016/j.spmi.2009.03.003>.
- [23] X. Zhang, G.J. Blanchard, Polymer sol-gel composite inverse opal structures, *ACS Appl. Mater. Interfaces.* 7 (2015) 6054–6061. <https://doi.org/10.1021/acsami.5b00656>.